IOPscience iopscience.iop.org

Home Search Collections Journals About Contact us My IOPscience

The interfacial free energy of solid Sn on the boundary interface with liquid Cd–Sn eutectic solution

This article has been downloaded from IOPscience. Please scroll down to see the full text article.

2007 J. Phys.: Condens. Matter 19 326219

(http://iopscience.iop.org/0953-8984/19/32/326219)

View the table of contents for this issue, or go to the journal homepage for more

Download details:
IP Address: 129.252.86.83
The article was downloaded on 28/05/2010 at 19:58

Please note that terms and conditions apply.

IOP PUBLISHING JOURNAL OF PHYSICS: CONDENSED MATTER

J. Phys.: Condens. Matter **19** (2007) 326219 (11pp) doi:10.1088/0953-8984/19/32/326219

The interfacial free energy of solid Sn on the boundary interface with liquid Cd–Sn eutectic solution

B Saatçi[1], S Çimen[2], H Pamuk[2] and M Gündüz[1]

[1] Department of Physics, Faculty of Arts and Sciences, Erciyes University, Talas Street 38039, Kayseri, Turkey
[2] Institute of Science, Erciyes University, Talas Street 38039, Kayseri, Turkey

Received 16 November 2006, in final form 21 May 2007
Published 17 July 2007
Online at stacks.iop.org/JPhysCM/19/326219

Abstract

Equilibrated grain boundary groove shapes for solid Sn in equilibrium with Cd–Sn liquid were directly observed after annealing a sample at the eutectic temperature for about 8 days. The thermal conductivities of the solid phase, K_S, and the liquid phase, K_L, for the groove shapes were measured. From the observed groove shapes, the Gibbs–Thomson coefficients were obtained with a numerical method, using the measured G, K_S and K_L values. The solid–liquid interfacial energy of solid Sn in equilibrium with Cd–Sn liquid was determined from the Gibbs–Thomson equation. The grain boundary energy for solid Sn was also calculated from the observed groove shapes.

1. Introduction

The solid–liquid interfacial energy, σ_{SL}, is defined as the reversible work required to create a unit area of the interface at constant temperature, volume and chemical potentials [1, 2], and it is an important physical parameter in nucleation, crystal growth from melt, welding phenomena, and liquid phase sintering. Unfortunately, the measurement of σ_{SL} is difficult. For this reason, values of σ_{SL} have usually had to be obtained either from nucleation theory [3–8], theoretical estimation [9–20], interpretation of crystal growth experiments [21–29], measurement of dihedral angles [30] and the direct applications of the Gibbs–Thomson equation (i.e. melting point of small crystal [31–35], and grain boundary groove shapes in an applied temperature gradient [36–50]).

One of the most common techniques used to measure σ_{SL} is to observe the equilibrated grain boundary groove shapes. In this technique, the solid–liquid interface is equilibrated with a grain boundary in a temperature gradient, G, as shown in figure 1; then it is necessary to accurately measure the shape of the grain boundary groove (cusps). The Gibbs–Thomson effect can be expressed in the form of the change in undercooling, ΔT_r, for an equilibrated grain boundary groove as

$$\Gamma = \Delta T_r r \tag{1}$$

 © 2007 IOP Publishing Ltd Printed in the UK

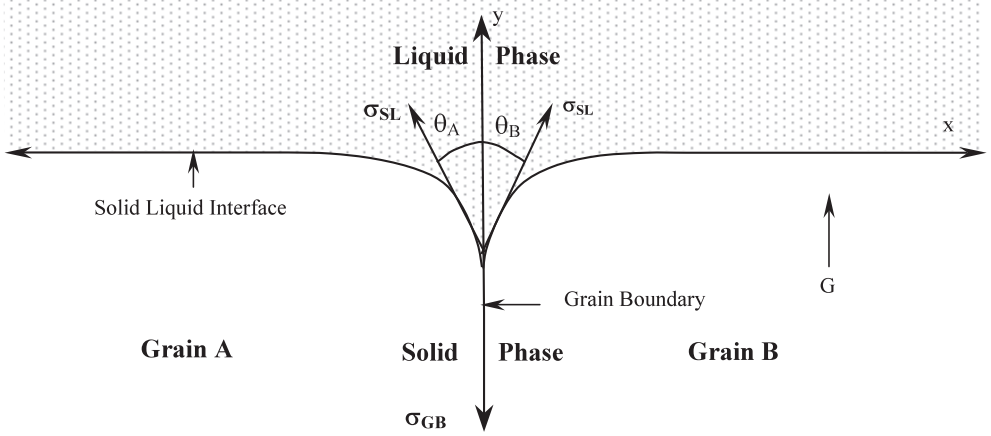

Figure 1. Schematic illustration of an equilibrated grain boundary groove formed at a solid–liquid interface in a temperature gradient, showing the x, y coordinates, $\vec{\sigma}_{SL}$, surface tension, $\vec{\sigma}_{GB}$, grain boundary tension and θ.

where Γ is the Gibbs–Thomson coefficient and r is the radius of the curved interface. Calculation of Γ values with equation (1) by using the equilibrated grain boundary groove shapes has been described in detail in the literature [41–50]. The solid–liquid interfacial energy is obtained from the thermodynamic definition of the Gibbs–Thomson coefficient, which is expressed as

$$\sigma_{SL} = \Gamma \Delta S^* \tag{2}$$

where ΔS^* is the effective entropy change per unit volume for melting. The solid–liquid surface energy can be obtained from equation (2) by using the calculated Γ values and known ΔS^* values.

The aim of the work is to determine Γ, σ_{SL}, and the grain boundary energy, σ_{GB}, of the solid Sn in equilibrium with the liquid Cd–Sn solution from the observed grain boundary groove shapes.

2. Experimental procedure

The experimental procedure and sample preparation were the same as in [45]. In this work a sample with initial concentration C_0 (Cd–95 at.% Sn alloy) was prepared in a vacuum furnace by using 99.99% pure Sn and 99.99% pure Cd. After several stirrings, the molten alloy was poured into a prepared graphite crucible held in a hot filling furnace which was set at approximately 50 K above the eutectic temperature, T_E, of the alloy (450 K). The molten metal was then directionally solidified in a hot filling furnace from bottom to top to ensure that the crucible was completely filled. The sample was then taken out of the hot filling furnace, all thermocouples and the inner heating element were placed in the sample, and the sample was inserted in a cooling jacket which was then was placed in the radial heat flow apparatus.

The sample was heated from the centre using a single wire and the outside of the specimen was kept cool with a water cooling jacket. A thin liquid layer (0.5–1 mm thick) was melted around the central heater and the specimen was annealed in a very stable temperature gradient for 8 days to get the equilibrated solid Sn with the Cd–Sn liquid. During the annealing period, the temperature of the stationary thermocouples was recorded continuously, and the

temperature of the moveable thermocouple and input power were periodically recorded. The temperature of the heating wire was controlled to an accuracy of ±0.05 K with a Eurotherm 905S type controller. The temperature in the sample was stable within about ±0.05 K for a day and ±0.1 K for up to a week. During the run, the specimen was kept in a slightly positive argon pressure. At the end of the annealing time, the sample was rapidly quenched by turning off the input power, which is sufficient to obtain a well-defined and stationary solid–liquid interface (i.e. grain boundary groove shapes) as shown in figure 2.

The quenched sample was first cut transversely into ∼25 mm length, and the transverse sections were ground flat with 180-grid SiC paper before mounting. Grinding and polishing were then carried out using standard metallographic techniques. After polishing, the samples were etched with a suitable enchant (10 ml acetic acid, 10 ml nitric acid, and 80 ml glycerin) to observe the equilibrated solid–liquid interface. The equilibrated grain boundary groove shapes which occurred on the solid–liquid interface were carefully photographed and numbered (figure 2). The groove shapes were selected from apparently larger grains on the longitudinal and transverse sections, and the symmetrical groove shapes were used for Γ determinations.

The actual coordinates of the cups, x, y, should be measured on orthogonal axes, x, y, z, where the x-axis is parallel to the solid–liquid interface, the y-axis is normal to the solid–liquid interface and the z-axis lies at the base of the grain boundary groove. Maraşli and Hunt [43] showed that measured x', y' coordinates can be transformed to x, y coordinates by considering the geometry of the grain boundary groove shapes in two different planes which are parallel to each other (see the details in [43]). The relation between x and x' can be expressed as [43]

$$x = x' \cos\alpha = x' \frac{\sqrt{a^2 + d^2}}{\sqrt{a^2 + b^2 + d^2}} \tag{3}$$

and the relation between y' and y can be expressed as

$$y = y' \cos\beta = y' \frac{d}{\sqrt{a^2 + d^2}} \tag{4}$$

where d is the distance between the first and second plane along the z'-axis, b is the displacement of the grain boundary position along the x'-axis, a is the displacement of the solid–liquid interface along the y'-axis, α is the angle between the x'-axis and x-axis, and β is the angle between the y'-axis and y-axis.

As can be seen from equations (3) and (4), if the values of a, b and d are measured, then the groove coordinates, x', y', can be transformed into x, y coordinates.

When the thermal conductivity of the solid phase, K_S, is not equal to the thermal conductivity of the liquid phase, K_L, the curvature undercooling, ΔT_r, is no longer a linear function of the distance. In order to calculate the Gibbs–Thomson coefficient, Γ with a numerical method, it is necessary to know the thermal conductivity of both phases. The thermal conductivity of the phases must be measured as accurately as possible not only to find out the thermal conductivity ratios ($R = K_L/K_S$) but also to calculate the temperature gradient, G_S, in the solid phase at the solid–liquid interface.

The radial heat flow is an ideal technique for measuring the conductivities of the solid phases. The temperature gradient is given by the Fourier law as

$$G_S = \left(\frac{dT}{dr}\right) = -\frac{Q}{AK_S}. \tag{5}$$

Integration of equation (5) for the radial heat flow gives

$$K_S = \frac{Q \ln(r_2/r_1)}{2\pi\ell(T_1 - T_2)} \tag{6}$$

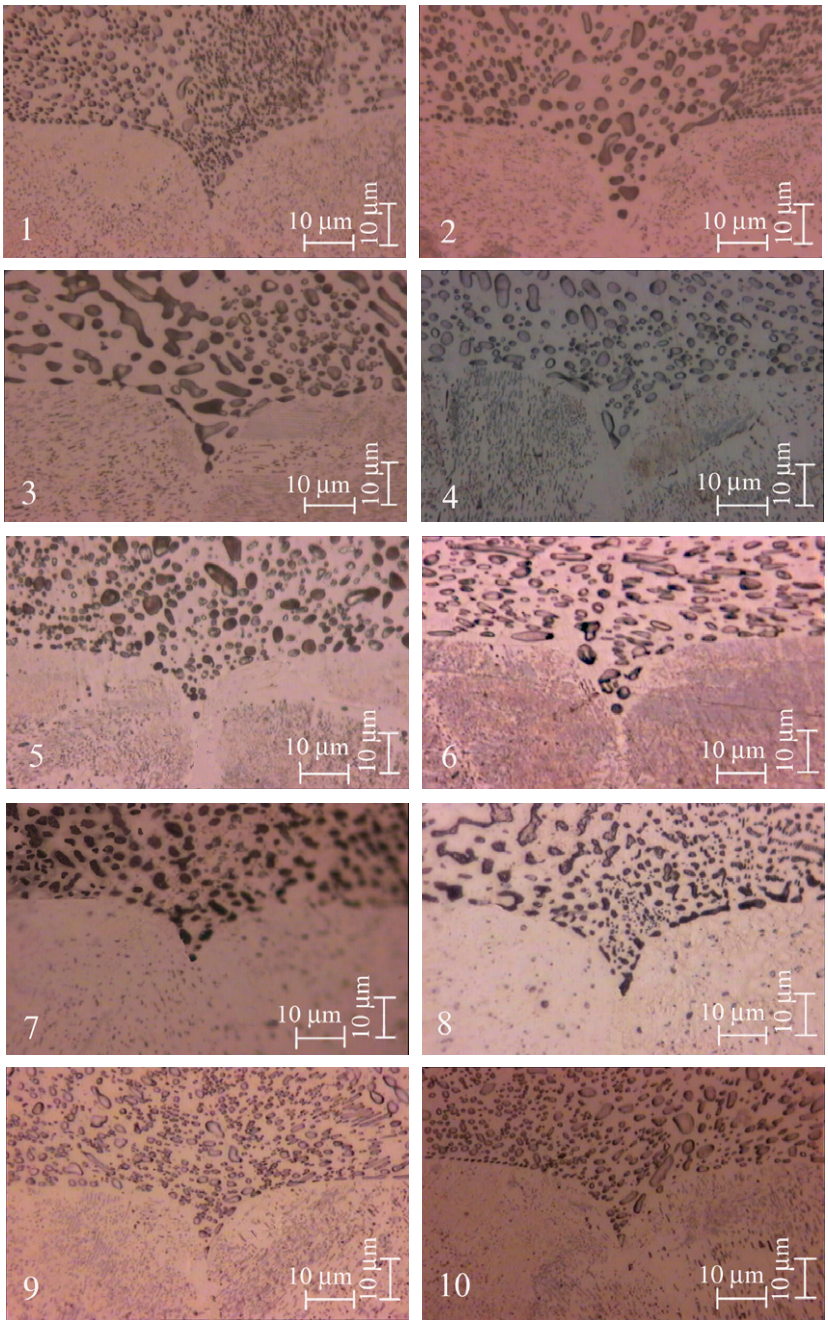

Figure 2. Typical grain boundary groove shapes for the solid Sn in equilibrium with liquid Cd–Sn solution.

(This figure is in colour only in the electronic version)

where Q is the input power from the centre of the sample, ℓ is the length of the heating element, r_1 and r_2 are fixed distances from the centre of the sample, and T_1 and T_2 are temperatures at

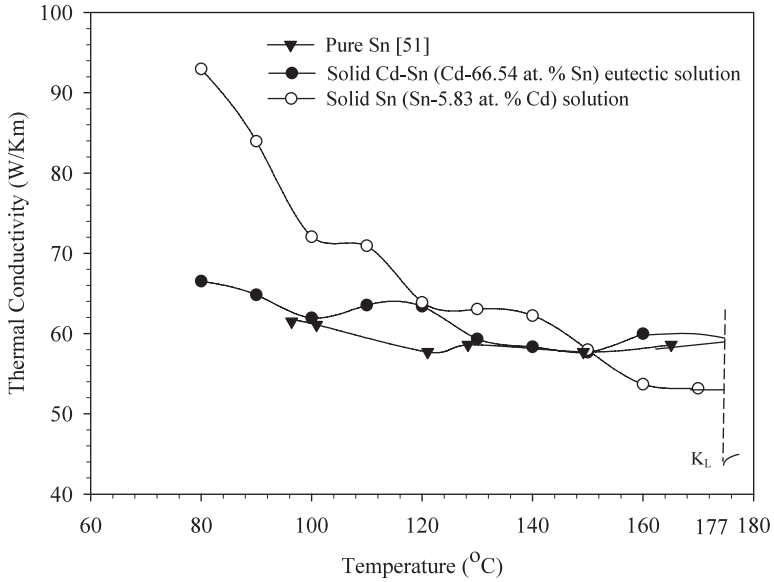

Figure 3. Thermal conductivities of pure Sn [51], solid Sn solution and solid Cd–Sn eutectic solution.

the fixed positions r_1 and r_2, respectively. If Q, ℓ, r_1, r_2, T_1 and T_2 can be accurately measured for a well-characterized sample, then reliable K_S values can be evaluated.

The sample was heated up in steps of 20 K up to 445 K (5 K below T_E). First, isotherms macroscopically parallel to the axial centre of the sample were obtained for the desired temperature, by moving the central heater up and down, and the sample was kept at this steady-state condition for at least 2 h. Then total input power Q and T_1, T_2 temperatures were measured at this condition. Finally, the sample was left to cool to room temperature. Then the sample was moved from the radial heat flow apparatus and was cut transversely near to the measurement points. After that the sample was ground and polished for r_1 and r_2 measurements. The distance was measured with Olympus HP2 optical microscope to an accuracy of ± 0.01 mm. The transverse and longitudinal sections of the sample were examined for porosity, cracks and casting defects to make sure that these would not introduce any errors to the measurements.

The thermal conductivities of solid phases of Cd–66.54 at.% Sn (Cd–Sn eutectic) and Sn–5.83 at.% Cd alloys were measured in the radial heat flow apparatus and are shown in figure 3. As can be seen from figure 3, in order to obtain the K_S values at T_E, the thermal conductivity versus temperature curves were extrapolated to the eutectic temperature, T_E. The value of thermal conductivity of the solid Sn solution, K_S, and the thermal conductivity of the solid Cd–Sn eutectic solution are obtained as 53 W K^{-1} m^{-1} and 60 W K^{-1} m^{-1}, respectively. The liquid thermal conductivity to solid thermal conductivity ratio ($R^E = K_L^E/K_S^E$) for the Cd–Sn eutectic solution was obtained from a directional solidification experiment as 0.73. The value of thermal conductivity of the liquid Cd–Sn eutectic solution, K_L, is obtained as 44 W K^{-1} m^{-1} by using the measured K_S and R^E values. So, the thermal conductivity ratio $R = K_L/K_S$ is obtained as 0.83 for solid Sn in equilibrium with liquid Cd–Sn solution.

The temperature gradient, G_S, at the solid–liquid interface in the solid phase was calculated for each grain boundary groove, by using the thermal conductivity of the solid phase, the input power, the length of the heating element, and the position of the solid–liquid interface.

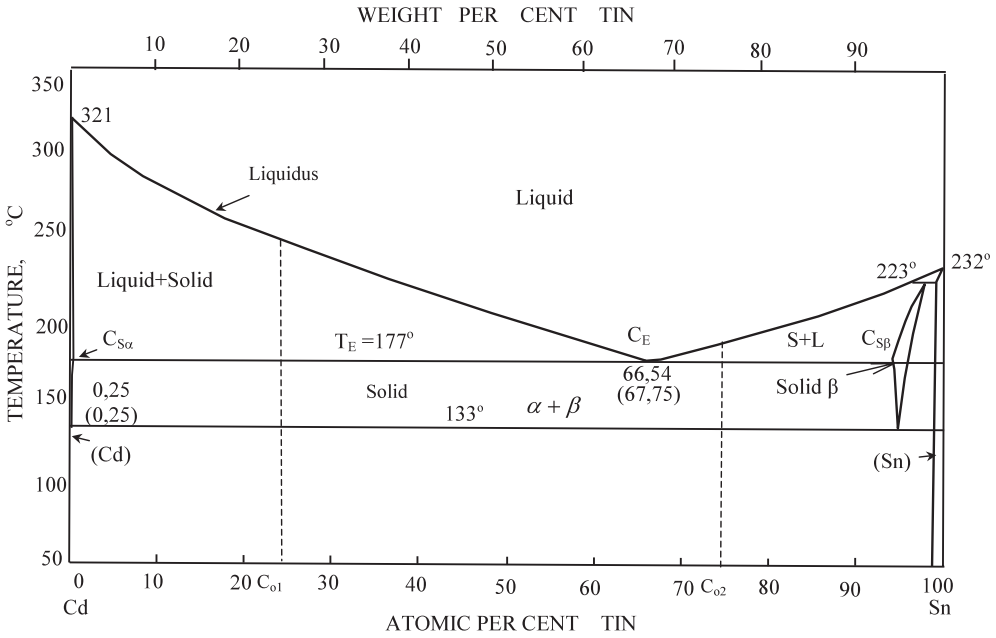

Figure 4. Cd–Sn phase diagram [52].

3. Results and discussion

If a binary eutectic alloy is held in a temperature gradient above the eutectic temperature with a composition of C_0 (provided that $C_{S\alpha} < C_0 < C_E$ or $C_E < C_0 < C_{S\beta}$), initially the alloy will be a mixture of solid and liquid up to the liquidus temperature (figure 4) [52]. In the sample, liquid will be present not only in the solid phase as a droplet but also in the grain boundary as liquid channels. The existence of a temperature gradient will impose a composition gradient. This composition gradient provides the driving force for the interfacial movement. Each droplet and liquid channel transport solute into the bulk liquid according to temperature gradient zone melting (TGZM) [53–56].

Cleaning up the grain boundaries takes longer than the droplet migrating into the bulk liquid through the solid. This is due to the possibility of some liquid droplet addition to the liquid channel and because of the effect of curvature of the cusp on the driving force of the interface motion. The TGZM processes will be completed when the uniform liquid phase (which is almost of the eutectic composition C_E, at the interface) has a sharp solid–liquid interface with the single solid phase (which is a composition almost at the limit of solid solubility, C_S). The phases will not be completely uniform because of the temperature gradient which produces a small compositional gradient in an alloy system at equilibrium. Mass transport by thermal diffusion (Sorét effect) and segregation become especially significant in large phases for high temperature gradients. The concentration change in the liquid phase and single solid phase has been calculated and obtained by chemically analysis for the Pb–Sn system [57]. It has been shown that the concentration change due to a 2 K temperature difference for the 1 mm Pb–Sn liquid layer was found to be in the order of 0.001 at fraction 0.1 atomic percent. The concentration change was even smaller than this value for a thinner liquid layer, i.e. there was no detectable Sorét effect and segregation effect in the equilibrated liquid and solid phases.

Table 1. Gibbs–Thomson coefficients for solid Sn in equilibrium with liquid Cd–Sn solution.

				Gibbs–Thomson coefficient $\times 10^{-8}$ (K m)	
Groove no. (see figure 2)	$G \times 10^2$ (K m^{-1})	α (deg)	β (deg)	LHS of the groove	RHS of the groove
1	7.01	3.3	1.7	6.49	7.42
2	7.37	35.5	10.5	7.43	7.76
3	7.84	2.5	26.5	6.16	6.67
4	7.71	4.0	4.1	6.76	8.69
5	7.17	3.2	3.1	6.68	7.53
6	7.41	1.9	3.0	8.31	8.00
7	8.73	3.9	3.3	7.30	7.43
8	7.68	6.8	16.7	7.20	7.71
9	7.23	4.7	1.7	6.40	6.90
10	6.53	10.0	13.3	7.40	7.31

A small temperature decrease causes solidification at the equilibrated solid–liquid interface and also at the solid phase-casting region interface, and a small temperature increase causes melting at same interfaces. The later effect causes new liquid droplets to join the single solid phase and the grain boundaries. Both solidification and melting prevent the solid–liquid interface from becoming stationary and thus the phases reaching equilibrium. Non-equilibrated grooves (because of the small temperature fluctuation or short annealing time) have liquid droplets in the single solid phase and/or liquid films in the grain boundaries. These effects can be minimized by using a very stable temperature gradient for a long enough time. The equilibrated grain boundary grooves will then be stationary, and the solid phase and the grain boundaries will not be contaminated with droplets or liquid films. So, equilibrated grain boundary groove shapes are formed, where the planar grain boundaries intersect with the stabilized planar solid–liquid interface. The equilibrated grain boundary groove shapes should be selected from apparently large and symmetrical grains with a thin liquid layer for Γ calculations in order to prevent errors from the Sorét effect and/or segregation effect.

The Gibbs–Thomson coefficient, Γ, can be calculated by a numerical method for any equilibrated grain boundary groove shape provided that the thermal conductivities of the phases, K_S, K_L, the temperature gradient, G, of the solid phase at the solid–liquid interface and the actual coordinates of the grooves (x, y) are known. The Gibbs–Thomson coefficient for solid Sn in equilibrium with liquid Cd–Sn solution was determined from the equilibrated groove shapes by such a numerical method. The calculations of Γ were made using ten equilibrated grain boundary groove shapes (figure 2) and the results are given in table 1. The average value obtained from table 1 is $\Gamma = 7.3 \times 10^{-8}$ K m with a standard deviation of $\pm 0.6 \times 10^{-8}$ K m. The estimated error in Γ obtained by considering the fractional error in each of the measured quantities was estimated to be in the order of 7–8%, which is similar to the scatter in the values calculated in table 1.

To calculate the solid–liquid interfacial energy, it is also necessary to know the effective entropy change per unit volume, ΔS^*. The effective entropy change for a two-component system is given as [41]

$$\Delta S^* = \frac{RT_E(C_S - C_L)}{m_L V_S (1 - C_L) C_L} \tag{7}$$

where R is the gas constant, T_E is the melting temperature of the alloy, V_S is the molar volume of solid, m_L is the liquidus slope, and C_S and C_L are the compositions of the equilibrated solid and liquid phases. The other parameters (T_E, m_L, C_S and C_L) can be obtained from the relevant

Table 2. Effective entropy change per unit volume ΔS^*, for solid Sn in equilibrium with liquid Cd–Sn solution.

Alloy	Liquid phase C_L	Solid phase C_S	$f(C)$	T_E (K)	$V_S \times 10^{-6}$ (m^3)	$m_L \times 10^2$ (K/at.fraction)	$\Delta S^* \times 10^6$ (J K^{-1} m^{-3})
Cd–Sn	Eutectic (Cd–66.54 at.%Sn)	Solid Sn (Sn–5.83 at.% Cd)	1.24	450	16.28	1.42	2.0

$f(C) = C_S - C_L/[(1 - C_L)C_L]$

Table 3. The solid–liquid interfacial energy for solid Sn in equilibrium with liquid Cd–Sn solution.

Alloy	Liquid phase	Solid phase	The Gibbs–Thomson coefficient $\Gamma \times 10^{-8}$ (K m)	Effective entropy change $\Delta S^* \times 10^6$ (J K^{-1} m^{-3})	The solid–liquid interfacial energy σ_{SL} (mJ m^{-2})
Cd–Sn	Eutectic (Cd–66.54 at.% Sn)	Solid Sn (Sn–5.83 at.% Cd)	7.3 ± 0.6	2.0	146 ± 11

phase diagram (figure 4). The values used to calculate the effective entropy change per unit volume for Cd–Sn eutectic system are given in table 2. The error in the determined m_L is about 4% [58]. The estimated error in the effective entropy change per unit volume obtained by considering the fractional error in each of the measured quantities was estimated to be of the order of 5%.

If the Gibbs–Thomson coefficient, Γ, and the effective entropy change, ΔS^*, are known or measured, the solid–liquid interfacial energy, σ_{SL}, can be calculated from equation (2) for any system. The values of σ_{SL} together with the estimated errors and standard deviation are given in table 3. The error in Γ was estimated to be 8% and in ΔS^* about 5%, and this gave a total estimated error of 13%. A comparison with the previous work is shown in table 4(b). A reasonably good agreement is obtained between the experimental values of σ_{SL} of solid Sn in equilibrium with liquid Cd–Sn solution (146 mJ m^{-2}) and solid Sn in equilibrium with liquid Pb–Sn solution (132.43 mJ m^{-2}). However, σ_{SL} values for Sn (49, 54.5, 59, 59.3, 62, 65, 70.6 and 77 mJ m^{-2}) obtained with the homogenous nucleation theory by Mondal [59], Turnbull [3], Eustathopoulos [15], Skripov [60], Waseda [12], Lu [67], Turnbull [4], Perepezko *et al* [8], and Vinet *et al* [61] respectively are rather smaller than our experimental result for the solid Sn–liquid Cd–Sn solution. Values of σ_{SL} for pure Sn (44, 50, 53.6, 60, 62 and 66 mJ m^{-2}) obtained with the theoretical estimates by Kotze and Kuhlmann-Wilsdorf [13], Jones and Chadwick [56], Waseda *et al* [12], Zadumkin [10], Lu *et al* [62] and Miedema [19] are also smaller than our experimental results. Solid–liquid interfacial energy values obtained with the crystal growth (CG) method by Jordan and Hunt [28], with the depression melting point (DMP) method by Wronski [32] and Waseda [12] and with nucleation undercooling (NU) method by Jones [63] and Eustathopoulos [68] are also smaller than our experimental result (table 4). It should be noted that the nucleation theory will give lower values, and also that nucleation theory only considers pure materials (i.e. both the solid phase and the liquid phase have the same pure materials); it should also be noted that the effect of alloying for the solid phase, liquid phase or both phases will probably increase the solid–liquid interfacial energy due to the actual alloy addition as well as due to the decrease in temperature.

From the force balance at the grain boundary groove, the grain boundary energy can be expressed as

$$\sigma_{GB} = 2\sigma_{SL} \cos\theta, \tag{8}$$

Table 4. A comparison of σ_{SL}, and σ_{GB}, measured in the present work with the previous work. (Note: GBG: grain boundary groove method; CG: crystal growth; NU: nucleation under cooling; DMP: depression melting point.)

(a) For alloy systems: Sn-based binary alloys

System	Solid phase	Liquid phase	T_E (K)	Solid–liquid interfacial energy σ_{SL} (mJ m^{-2})	Grain boundary energy σ_{GB} (mJ m^{-2})
Cd–Sn	Sn (Sn–5.83 at.% Cd)	CdSn(Cd–66.54 at.% Sn)	450	146 ± 11 GBG [present work]	283 ± 40 GBG [present work]
Pb–Sn	Sn (Sn–1.45 at.% Pb)	PbSn (Sn–26.1 at.% Pb)	456	132.43 ± 17.22 [41] GBG	262.77 ± 36.79 [41] GBG

(b) For pure Sn

	Solid–liquid interfacial energy σ_{SL} (mJ m^{-2})			
System	Nucleation	Theoretical estimates	Experimental	Grain boundary energy σ_{GB} (mJ m^{-2})
Pure Sn	54.5 [3]	60 [10]	49.5–61.3 [28] from CG	160 [65]
	65 [4]	53.6 [12]	62 ± 10 [32] from DMP	164 [66]
	70.6 [8]	44 [13]	75 [63] from NU	
	59.3 [12]	66 [19]	83 [63] from NU	
	49 [59]	62 [62]	54 [63] from NU	
	59 [15, 60]	50 [64]	66 [63] from NU	
	77 [61]		66.2 [12] from DMP	
	62 [67]		62 [68] from NU	

where $\theta = \frac{\theta_A+\theta_B}{2}$ is the angle that the solid–liquid interface makes with the y-axis (figure 1). The angles, θ_A and θ_B, were obtained from the cusp coordinates, x and y, by using a Taylor expansion for the base of the groove. The grain boundary energies were calculated from equation (8) using the related σ_{SL} and θ for ten groove shapes for solid Sn in equilibrium with liquid Cd–Sn solution (figure 2) and given in table 4 and compared with results from previous work in the same table. The average grain boundary energy, with experimental error, was found to be $\sigma_{GB} = 283 \pm 40$ mJ m^{-2}. The error is estimated to be about 14% for σ_{GB}. A comparison of σ_{SL} and σ_{GB} measured in the present work with the previous work is given in table 4.

4. Conclusions

(1) The variation of the thermal conductivity with temperature up to T_E for the solid Sn and solid Cd–Sn eutectic solution was measured and the thermal conductivity of the liquid Cd–Sn eutectic solution at T_E was obtained for the Cd–Sn system.
(2) The equilibrated grain boundary groove shapes were obtained for solid Sn in equilibrium with liquid Cd–Sn solution with a radial heat flow apparatus, and the Gibbs–Thomson coefficient, Γ, was obtained by using the groove shapes as $\Gamma = (7.3 \pm 0.6) \times 10^{-8}$ K m.
(3) The effective entropy change per unit volume, ΔS^*, was calculated to be (2.0×10^6 J K^{-1} m^{-3}) by using the phase diagrams and related parameters.
(4) The solid–liquid interfacial energy, σ_{SL}, was measured to be $\sigma_{SL} = (146 \pm 11)$ mJ m^{-2} by using the Gibbs–Thomson coefficient, Γ, and the effective entropy change, ΔS^*.
(5) The grain boundary energies, σ_{GB}, were determined to be $\sigma_{GB} = (283 \pm 40)$ mJ m^{-2} by using the equilibrated groove shapes and the related σ_{SL}.

Acknowledgments

This project was supported by the Erciyes University Research Foundation under contract no. FBT-04-11. The authors are grateful to the Erciyes University Research Foundation for their financial support.

References

[1] Woodruff D P 1973 *The Solid–Liquid Interface* vol 36 (Cambridge: Cambridge University Press) pp 1–2
[2] Trivedi R 1999 *Lectures on the Theory of Phase Transformations* 2nd edn, ed H I Aaronson (New York: TMS-AIME) pp 135–64
[3] Turnbull D J 1950 *J. Chem. Phys.* **18** 768–75
[4] Turnbull D J 1949 *J. Appl. Phys.* **20** 817–24
[5] Skripov V P 1977 *Crystal Growth and Materials* ed E Kaldis and H Schell (Amsterdam: North-Holland) p 327
[6] Stowell M J 1970 *Phil. Mag.* **22** 1–6
[7] Glicksman M E and Vold C I 1969 *Acta Metall.* **17** 1–4
[8] Perepezko J H, Rasmussen H K, Anderson I E and Loper C R Jr 1979 *Solidification and Casting of Metals* The Metal Society, pp 169–74
[9] Skapski A S 1956 *Acta Metall.* **4** 576–82
[10] Zadumkin S N 1962 *Fiz. Met. Metalloved.* **13** 24
Zadumkin S N 1962 *Phys. Met. Metallogr.* **13** 24 (Engl. Transl.)
[11] Ewing R H 1971 *J. Cryst. Growth* **11** 221–4
[12] Waseda Y and Miller W A 1975 *Trans. Japan. Inst. Met.* **19** 546–52
[13] Kotze I A and Kuhlmann-Wilsdorf D 1966 *Appl. Phys. Lett.* **9** 96
[14] Miller W W and Chadwick S A 1967 *Acta Metall.* **15** 607–14
[15] Eustathopoulos N 1983 *Int. Metall. Rev.* **28** 189–209
[16] Eustathopoulos N, Joud J C and Dersé J 1972 *J. Chim. Phys.* **69** 69
[17] Eustathopoulos N, Joud J C and Dersé J 1974 *J. Chim. Phys.* **71** 777–87
[18] Waren R 1980 *J. Mater. Sci.* **15** 2489–96

[19] Miedema A R and Broeder F J A 1979 *Z. Metallk.* **70** 14–20
[20] Nason D and Tiller W A 1973 *Surf. Sci.* **40** 109–24
[21] Kirkaldy J S and Sharma R C 1980 *Acta Mater.* **28** 1009–21
[22] Hardy S C and Coriell S R 1969 *J. Cryst. Growth* **5** 329–37
[23] Hardy S C and Coriell S R 1968 *J. Cryst. Growth* **3–4** 569–73
[24] Hardy S C, Coriell S R and Sekerka R F 1971 *J. Cryst. Growth* **11** 53–67
[25] Trivedi R 1970 *Acta Metall.* **18** 287–96
[26] Miller-Klubhaar H and Langer J S 1978 *Acta Metall.* **26** 1697–708
[27] Glicksman M E and Schaefer R J 1968 *J. Cryst. Growth* **1** 297–310
[28] Jordan R M and Hunt J D 1971 *Metall. Trans.* **2** 3401–10
[29] Hunt J D 1979 *Solidification of Casting Metal* Metal Society, pp 3–9
[30] Glicksman M E and Vold C I 1971 *Scr. Metall.* **5** 493–8
[31] Coombes C 1972 *J. Phys. F: Met. Phys.* **2** 441
[32] Wronski C R M 1967 *Br. J. Appl. Phys.* **18** 1731–7
[33] Kubelka P and Prolscha R 1944 *Z. Kolloid* **109** 79
[34] Puri B R, Sharma L R and Lakhompal M L 1954 *J. Chem. Phys.* **58** 289–92
[35] Puri B R, Singh D D and Myer Y P 1957 *Trans. Faraday Soc.* **53** 530–4
[36] Bolling G F and Tiller W A 1960 *J. Appl. Phys.* **31** 1345–50
[37] Nash G E and Glicksman M E 1971 *Phil. Mag.* **24** 577–92
[38] Jones D R H and Chadwick G A 1970 *Phil. Mag.* **22** 291–300
[39] Jones D R H 1970 *Rew. Sci. Inst.* **41** 1509–11
[40] Hardy S C 1977 *Phil. Mag.* **35** 471–84
[41] Gündüz M and Hunt J D 1985 *Acta Mater.* **9** 1651–72
[42] Gündüz M and Hunt J D 1989 *Acta Mater.* **7** 1839–45
[43] Maraşli N and Hunt J D 1996 *Acta Mater.* **44** 1085–96
[44] Maraşli N, Keşlioğlu K and Arslan B 2003 *J. Cryst. Growth* **247** 613–22
[45] Saatçi B and Pamuk H 2006 *J. Phys.: Condens. Matter* **18** 10143–55
[46] Bayender B, Maraşli N, Çadırlı E, Şişman H and Gündüz M 1998 *J. Cryst. Growth* **194** 119–24
[47] Bayender B, Maraşli N, Çadırlı E and Gündüz M 1999 *Mater. Sci. Eng.* A **270** 343–8
[48] Keşlioğlu K, Erol M, Maraşli N and Gündüz M 2004 *J. Alloys Compounds* **385** 207–13
[49] Ocak Y, Akbulut S, Böyük U, Erol M, Keşlioğlu K and Maraşli N 2006 *Thermochim. Acta.* **445** 86–91
[50] Keşlioğlu K and Maraşli N 2004 *Mater. Sci. Eng.* A **369** 294–301
[51] Touloukian Y S, Powell R W, Ho C Y and Klemens P G 1970 Thermal conductivity metallic elements and alloys *Thermophysical Properties of Matter* 1 (Newyork: Plenum) pp 388–408
[52] Hansen M and Anderko K 1985 *Constitutions of Binary Alloys* 2nd edn (New York: McGraw-Hill) p 38
[53] Pfann W G 1956 *Trans. AIME* **20** 961–4
[54] Allen D J and Hunt J D 1979 *Solidification and Casting of Metals* (London: Metals Society) p 39
[55] Jones D R H 1972 *J. Cryst. Growth* **16** 187
[56] Jones D R H and Chadwick G A 1971 *Phil. Mag.* **24** 1327
[57] Gündüz M and Phil D 1984 *Thesis* University of Oxford
[58] Tassa M and Hunt J D 1976 *J. Cryst. Growth* **34** 38–48
[59] Mondal K and Murty B S 2007 *Mater. Sci. Eng.* A **454/455** 654–61
[60] Skripov V P 1977 Homogeneous nucleation in metals and amorphous films *Crystal Growth and Materials* ed E Kaldis and H Schell (Amsterdam: North-Holland) p 327
[61] Vinet B, Magnusson L, Fredriksson H and Desre P J 2002 *J. Colloid. Interface Sci.* **255** 363
[62] Lu H M, Wen Z and Jiang Q 2002 *Mater. Lett.* **53** 364–6
[63] Jones H 2002 *Mater. Lett.* **4–5** 364–6
[64] Digilov R M 2004 *Surf. Sci.* **555** 68–74
[65] Greenhill B E and McDonald S R 1953 *Nature* **171** 37
[66] Imman M C and Tipler H R 1963 *Metals. Rev.* **8** 105
[67] Lu H M, Wen Z and Jiang Q 2006 *Colloids Surf.* A **278** 160–5
[68] Eustathopoulos N and Joud J C 1980 Interfacial tension and adsorption of metallic systems *Curr. Topics Mater. Sci.* vol 4, ed E Kaldis (Amsterdam: North-Holland) p 281